Biosensors and Bioelectronics 173 (2021) 112800

Contents lists available at ScienceDirect

Biosensors and Bioelectronics

journal homepage: http://www.elsevier.com/locate/bios

An impedance biosensor based on magnetic nanobead net and MnO_2 nanoflowers for rapid and sensitive detection of foodborne bacteria

Li Xue [a], Ruya Guo [b], Fengchun Huang [b], Wuzhen Qi [a], Yuanjie Liu [a], Gaozhe Cai [b], Jianhan Lin [a,b,*]

[a] Key Laboratory of Agricultural Information Acquisition Technology, Ministry of Agriculture and Rural Affairs, China Agricultural University, Beijing, 100083, China
[b] Key Laboratory of Modern Precision Agriculture System Integration Research, Ministry of Education, China Agricultural University, Beijing, 100083, China

ARTICLE INFO

Keywords:
Impedance biosensor
Magnetic nanobead net
Large-volume magnetic separation
MnO_2 nanoflowers
Salmonella detection

ABSTRACT

Screening of pathogenic bacteria in foods is an effective way to prevent foodborne diseases. In this study, an impedance biosensor was developed for rapid and sensitive detection of *Salmonella typhimurium* using multiple magnetic nanobead (MNB) nets in a ring channel for continuous-flow separation of target bacteria from 10 mL of sample, manganese dioxide nanoflowers (MnO_2 NFs) for efficient amplification of biological signal, and an interdigitated microelectrode for sensitive measurement of impedance change. First, the MNBs modified with capture antibodies were vortically injected from outer periphery of this ring channel to form multiple ring MNB nets at specific locations with high gradient magnetic fields. Then, the bacterial sample was continuous-flow injected, resulting in specific capture of target bacteria onto the nets, and the MnO_2 NFs modified with detection antibodies were injected to form MNB-bacteria-MnO_2 NF complexes. After the complexes were washed with deionized water to remove excessive nanoflowers and residual ions, H_2O_2 with poor conductivity was injected to reduce MnO_2 NFs to conductive Mn^{2+} at neutral medium, leading to impedance decrease. Finally, impedance change was measured using the microelectrode for quantitative determination of *Salmonella*. This biosensor was able to separate ~60% of *Salmonella* from 10 mL of bacterial sample and detect *Salmonella* with a linear range of 3.0×10^1 to 3.0×10^6 CFU/mL in 1.5 h with lower detection limit of 19 CFU/mL. This biosensor might be further improved with higher sensitivity using a larger volume (100 mL or more) for routine screening of foodborne bacteria without bacterial pre-culture.

1. Introduction

Foodborne diseases caused by pathogenic bacteria have increasingly become a worldwide concern due to serious public health issues and considerable economic losses (Jung et al., 2020; Wang et al., 2020c). An effective way to prevent the outbreaks of foodborne diseases is rapid and accurate screening of pathogenic bacteria in whole food supply chains. Conventional approaches for bacterial detection mainly include culture plating (Culture), enzyme-linked immunosorbent assay (ELISA) and polymerase chain reaction (PCR). However, Culture is time-consuming; conventional ELISA lacks sensitivity and PCR requires complex DNA extraction (Abdelhaseib et al., 2016; Pang et al., 2018; Shan et al., 2016; Zhou et al., 2016). Thus, various biosensors, including electrochemical (Cesewski and Johnson 2020; Mathelié-Guinlet et al., 2019), optical (Du et al., 2020; Hu et al., 2019) and piezoelectric (Yang et al., 2019), have been developed for rapid detection of foodborne bacteria. Impedance biosensor is a major branch of electrochemical biosensors, which relies on the measurement of electrochemical impedance change on the interface of an electrode under an alternating perturbation with a constant bias, and has shown the merits of compact design, rapid response, relatively low cost, and easy integration in the detection of foodborne bacteria (Helali et al., 2018; Jasim et al., 2019).

The procedure for routine screening of pathogenic bacteria in foods generally includes sample collection, bacteria separation and bacteria detection. Because food samples are usually very complex with low concentration of bacteria, specific separation and efficient concentration of target bacteria have received increasing attention in the development of biosensors for sensitive and accurate detection of bacteria. To date, some efforts have been made to develop new bacteria separation methods using magnetic beads (MBs) (Armbrecht et al., 2015;

* Corresponding author. Key Laboratory of Agricultural Information Acquisition Technology, Ministry of Agriculture and Rural Affairs, China Agricultural University, Beijing, 100083, China.
E-mail address: jianhan@cau.edu.cn (J. Lin).

https://doi.org/10.1016/j.bios.2020.112800
Received 9 August 2020; Received in revised form 14 October 2020; Accepted 3 November 2020
Available online 6 November 2020

Bezdekova et al., 2020; Jung et al., 2018; Lee et al., 2014; Pastucha et al., 2019). A recent study on immunomagnetic flow separation of pathogenic bacteria from a large volume (10 mL) of sample was reported using a 3D-printed cylindrical microchannel to capture immune MBs under an external magnetic field for specific reaction with continuously flowing target bacteria. Combined with Adenosine Tri-Phosphate (ATP) luminometer, this method could detect *E. coli* O157:H7 in 3 min with a low detection limit of 10 CFU/mL (Lee et al., 2014). However, a large amount of immune MBs (200 μg, around 10 times more than conventional magnetic separation) were required to ensure efficient capture of target bacteria, resulting in high cost for each test. In the past years, some studies on magnetic bead chains or net were reported to enhance the separation and concentration of bacteria. A typical study was reported by self-assembling the MBs into chain structure under a magnetic field, which was demonstrated to enhance active contact between the analyte and the MBs(Armbrecht et al., 2015). Recently, it is noteworthy that a magnetic nanobead virtual net was developed by Lee et al. based on Lenz's law for separation of pathogenic bacteria in a conductive microfluidic channel using a glass tube wrapped with a copper tape under an external magnetic field. Combined with ATP luminometer, it could detect *E. coli* O157:H7 in 15 min with a low detection limit of 10^2 CFU/mL (Lee et al., 2019a).

Except for specific separation and efficient concentration of target bacteria from complex backgrounds, signal amplification is another effective strategy to improve the sensitivity of biosensors. With fast advance of nanomaterials, many nanoflowers and nanocomposites have been successfully developed for signal amplification. Among them, the facile-to-synthesize and non-toxic manganese dioxide (MnO_2) nanosheets or nanoflowers with peroxidase-mimic characteristic have been intensively employed for optical (Han et al., 2019; Zhang et al., 2019) and amperometric (Shu et al., 2017; Xu et al., 2019) detection of different targets (Ouyang et al., 2018; Zhang et al., 2020). Besides, the MnO_2 nanosheets/nanoflowers could be reduced to Mn^{2+} at the presence of hydrogen peroxide (H_2O_2) in neutral medium (Huang et al., 2017; Lee et al., 2019b). However, to the best of our knowledge, the electrochemical impedance characteristic of MnO_2 has not been deeply investigated so far and reported for detection of bacteria. Thus, it might be promising to amplify electrochemical impedance signals using MnO_2 nanoflowers.

In our previous studies, some double-layer channels filled with iron balls, which were magnetized by inner or external repelling magnets, have been developed for relatively uniform capture of immune MBs to specifically and effectively separate different foodborne bacteria from large volume of food samples (Huang et al., 2018b; Wang et al., 2020b; Xue et al., 2018). Although the MBs were able to distribute relatively uniformly along the axial direction, the distribution of these MBs in the radical direction was still non-uniform because they were aggregated against the walls of ring channel, resulting in the blocking of partial MBs to react with target bacteria. Besides, in our very recent studies (Hou et al., 2020; Wang et al., 2020a), the forming of magnetic bead chains in the ring channels was demonstrated to effectively enhance the capture efficiency of target bacteria due to more occupation of MBs in the cross section, however the height of magnetic bead chains was limited (not higher than half of the ring channel's height) due to the homogeneous distribution of these MBs in the radical direction, resulting in the loss of partial bacteria to be captured by immune MBs. Thus, an impedance biosensor was developed in this study for rapid and sensitive detection of *Salmonella typhimurium* using magnetic nanobead nets for continuous-flow separation of target bacteria from a large volume (10 mL) of bacterial sample and MnO_2 nanoflowers for efficient amplification of biological signal. As shown in Fig. 1, the magnetic nanobeads (MNBs) modified with the capture antibodies (CAbs) against *Salmonella*

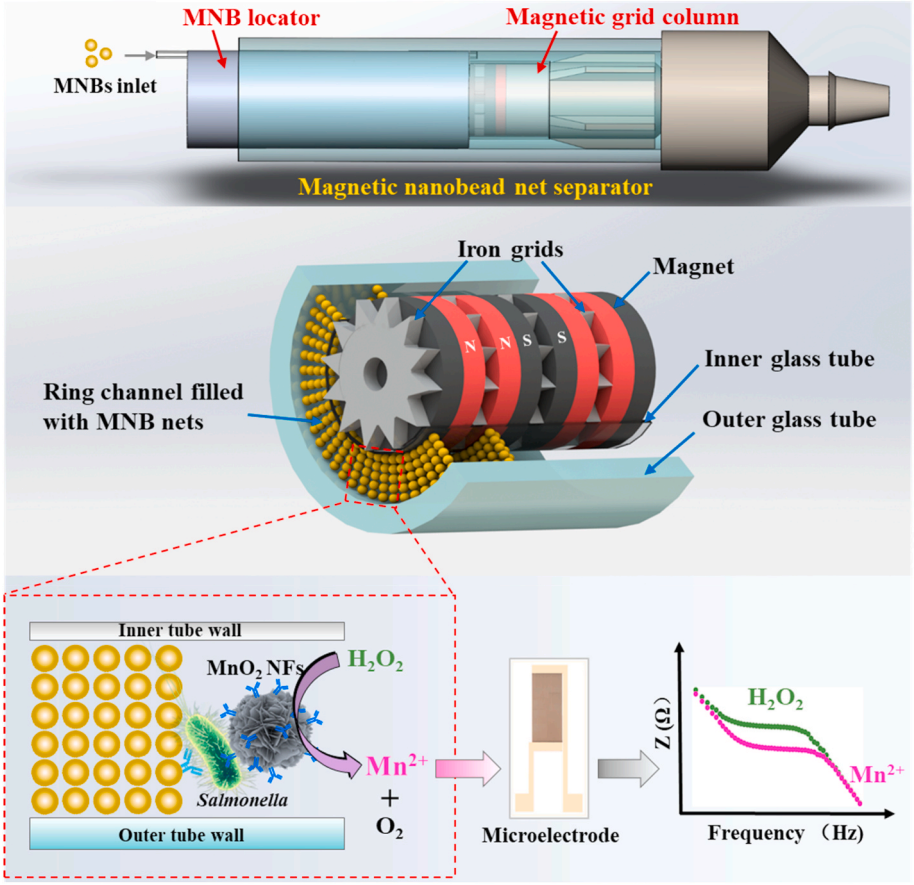

Fig. 1. Schematic of this impedance biosensor for detection of *Salmonella*.

were first vortically injected from the outer periphery of ring channel into the separation column using the newly-designed magnetic nanobead locator (MNB locator), resulting in the forming of multiple ring MNB nets around the tips of round iron gears. After a large volume (10 mL) of bacterial sample was continuous-flow injected into the channel, resulting in specific capture of target bacteria by the CAbs onto the MNB nets, the MnO_2 NFs modified with the detection antibodies (DAbs) were injected and conjugated with the target bacteria to form MNB-CAb--bacteria-DAb-MnO_2 NF complexes, which were washed with deionized water to remove excessive nanoflowers and residual ions. Finally, H_2O_2 with poor conductivity was injected to reduce the MnO_2 NFs on the complexes into Mn^{2+} with strong conductivity, leading to impedance decrease, and the impedance change was measured using the microelectrode to determine the concentration of target bacteria.

2. Materials and methods

2.1. Materials

The streptavidin-modified MNBs (150 nm, 1 mg/mL) from Ocean Nanotech (San Diego, CA, USA) were used for separating the target bacteria from sample. Hydrochloric acid (HCl) and polyvinylpyrrolidone (PVP) from Sigma Aldrich (St. Louis, MO, USA) and potassium permanganate ($KMnO_4$) from Sinopharm Chemical (Beijing, China) were used for synthesizing the MnO_2 NFs. 3-Aminopropyl triethoxysilane (APTES) from Aladdin (Shanghai, China) was used to functionalize the surface of MnO_2 NFs with the amino groups. Hydrogen peroxide (30%, v/v) from Aladdin was used for reducing the MnO_2 NFs to Mn^{2+}. The anti-Salmonella CAbs (2.5 mg/mL) from Abcam (Cambridge, MA, USA, Cat#: ab69255) and anti-Salmonella DAbs (2.85 mg/mL) from Meridian (Memphis, TN, USA, Cat#: C86309M) were used for specifically reacting with Salmonella, respectively. TCO-PEG4-NHS ester (TCO) and tetrazine-sulfo-NHS ester (Tz) from Click Chemistry Tools Bioconjugate Technology (Scottsdale, AZ, USA) were used for conjugating the detection antibodies onto the surface of MnO_2 NFs. Phosphate buffered saline (PBS, 10 mM, pH 7.4) from Solarbio (Beijing, China) was used as buffer solution. Bovine serum albumin (BSA, 1%, w/v) from EM Science (Gibbstown, NJ, USA) was prepared in PBS for blocking. Tween-20 from Amresco (Solon, OH, USA) was prepared in deionized water for washing. Other reagents were of analytical grade and purchased from Sinopharm Chemical. Deionized water produced by Advantage A10 from Millipore (18.2 MΩ cm, Billerica, MA, USA) was used for preparing all the solutions.

2.2. Fabrication of the magnetic nanobead net separator

The magnetic nanobead net separator is the most important component of this biosensor and has a significant impact on the separation efficiency of target bacteria. As shown in Fig. 1 and Fig. S1, this separator mainly included two parts: a MNB locator and a magnetic grid column. The magnetic grid column was composed of an inner glass tube (inner diameter: 4.5 mm, outer diameter: 5.5 mm) and an outer glass tube (inner diameter: 7.0 mm, outer diameter: 9.0 mm). Ten cylinder magnets (material: NdFeB; grade: N52; diameter: 4.0 mm; thickness: 1.5 mm) were assembled at mutual repelling layout in the inner glass tube and every two adjacent magnets were separated by a ring iron gear (diameter: 4.4 mm; thickness: 0.5 mm; gear number: 12) to generate local high gradient magnetic fields. One end of the inner tube was sealed and the other end was blocked and connected with a coaxial aligner, which was fabricated by a 3D printer (Object 24, Stratasys, Eden 152 Prairie, MN, USA). The inner tube was concentrically assembled inside the outer tube to form the ring channel. The newly-designed MNB locator consisted of a 3D-printed cylinder (inner diameter: 5.7 mm, outer diameter: 6.9 mm) and a Teflon tubing (inner diameter: ~0.3 mm, outer diameter: ~0.5 mm). The tubing for injecting the MNBs was assembled at the outer surface of the cylinder and located between the cylinder and the outer glass tube. When the outlet of the tubing was located at each iron gear, the MNBs were continuously injected into the tubing while the whole magnetic grid column was rotated slowly (~3 rpm). As a result, all the MNBs were continuous-flow injected from the outer wall of the ring channel and attracted by the high gradient magnetic field at the inner wall of the channel, resulting in their successive movement towards the iron gear in all directions and thus the forming of a MNB net around the gear in the ring channel. Multiple MNB nets were formed when the MNB locator was moved from one gear to another. Besides, each end of the outer glass tube was connected with a silicone hose via a 3D-printed connector. One silicone hose was installed on a peristaltic pump (T60-S2&WX10-14-A, Longer, Baoding, China) for accurate control of the fluids.

2.3. Synthesis of the immune MnO_2 NFs

The MnO_2 nanoflowers were synthesized and functionalized with amino groups based on our previous report with slight modifications (Xue et al., 2020). The detailed protocol for synthesis of the MnO_2 NFs could be found in the supplementary material and the TEM and SEM pictures of the MnO_2 NFs could be found in Fig. S2. The small molecules, Tz and TCO, were prepared in DMF with the concentration of 10 mM and used to conjugate the DAbs onto the surface of MnO_2 NFs via click chemistry (Huang et al., 2018a; Xianyu et al., 2018). First, the DAbs were functionalized with Tz by mixing the DAbs and the Tz reagent at a molar ratio of 1:40 and incubating for 45 min at room temperature. Then, the mixture was transferred into a centrifugal ultra-filter (10 kD) and centrifuged at 12,000 rpm for 20 min at 4 °C, followed by washing three times with deionized water to remove the residual Tz. Similarly, the MnO_2 NFs were functionalized with TCO by mixing the MnO_2 NFs and the TCO reagent and incubating for 45 min at room temperature, followed by centrifuging at 10,000 rpm for 10 min and washing three times with deionized water to remove the residual TCO. Finally, the TCO-functionalized MnO_2 NFs were mixed with the Tz-functionalized DAbs for 45 min to synthesize the immune MnO_2 NFs through the specific reaction between Tz and TCO.

2.4. Preparation of the bacterial samples

Salmonella typhimurium (ATCC14028) from American Type Culture Collection (ATCC) was used as target bacteria. *Listeria monocytogenes* (ATCC13932) and *Escherichia coli* O157:H7 (ATCC43888) from ATCC, and *Staphylococcus aureus* (CICC10001) and *Bacillus cereus* (CICC10041) from China Center of Industrial Culture Collection (CICC) were used as the non-target bacteria. All these bacterial strains were stored at −20 °C in a glycerol/broth medium (30%, v/v) and re-activated by incubating the bacteria in 5 mL of sterile Luria-Bertani (LB) medium (Aoboxing Biotech, Beijing, China) at 37 °C with shaking for 16–24 h. The bacterial cultures were 10-fold diluted with sterile PBS to obtain the bacteria at the concentrations of 10^1–10^6 CFU/mL, respectively. Bacterial enumeration was conducted using the standard culture plating.

2.5. Establishment of the calibration model

To establish the calibration model for this biosensor, 10 mL of the target bacterial samples with different concentrations ranging from 3×10^1 to 3×10^6 CFU/mL were prepared and detected using this biosensor. Prior to testing, the magnetic grid column and the MNB locator were successively rinsed with alcohol (75%, v/v) and deionized water, followed by blocking with 1% BSA for 30 min and washing with sterile PBS. First, 40 μg of the prepared immune MNBs in 200 μL of PBS, which were prepared according to our reported protocol (Huang et al., 2018b) and also could be found in the supplementary material, were injected into the ring channel at a flow rate of 20 μL/min using the MNB locator while the magnetic grid column was rotated at a speed of 3 r/min, and the immune MNB nets were formed around the iron grids one by one in the

ring channel. After the locator was removed and the silicone hoses were connected, 10 mL of target bacterial sample was injected into the channel and the target bacteria were captured onto the immune MNB nets to form the MNB-bacteria complexes (magnetic bacteria), followed by washing with deionized water. Then, 500 μL of the immune MnO_2 NFs (0.2 mg/mL) were injected and incubated with the magnetic bacteria for 45 min to form MNB-bacteria-MnO_2 NF complexes. After the complexes were successively washed with the deionized water containing 0.05% Tween-20 one time and deionized water three times to remove the excessive nanoflowers and residual ions, 500 μL of H_2O_2 (10 mM) was injected to reduce MnO_2 to Mn^{2+} for 15 min. Finally, the solution was flushed out, and its impedance was measured using the microelectrode on an electrochemical workstation (IM6, Zahner, Kronach, Bavaria, Germany) to determine the concentration of the target bacteria. After each measurement, the microelectrode was rinsed with the deionized water to remove the residual ions. The impedance change (ΔZ) at the characteristic frequency of 10 kHz was calculated as the difference between the impedance of H_2O_2 (Z_0) and that of bacterial sample (Z), i.e., $\Delta Z = Z_0 - Z$.

2.6. Detection of the target bacteria in chicken meats

Chicken meats purchased from the local supermarket were used as research model for detection of *Salmonella* in real food samples. The chicken meats were first prepared to obtain the supernatant according to China's food safety national standards on detection of pathogens in foods (GB 4789) (Xue et al., 2020). Then, pure *Salmonella* cultures were added into the supernatant to prepare the spiked samples with the bacterial concentrations of 5×10^1, 5×10^2 and 5×10^3 CFU/mL. Finally, three tests for each spiked sample were conducted in parallel using both this biosensor and the standard culture plating. The recovery (R) was calculated as the ratio of the readout (C_b) of this impedance biosensor to the result (C_p) of culture plating.

3. Results and discussion

3.1. Mechanism of this magnetic nanobead net separation

The forming of magnetic nanobead nets is crucial for efficient separation of target bacteria from large volume of sample. Thus, it is of great importance to understand the forming mechanism of MNB nets. As shown in Fig. 2(a), when a MNB is injected from the MNB locator into

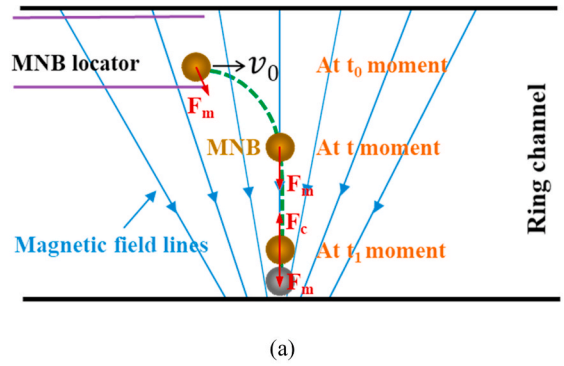

(a)

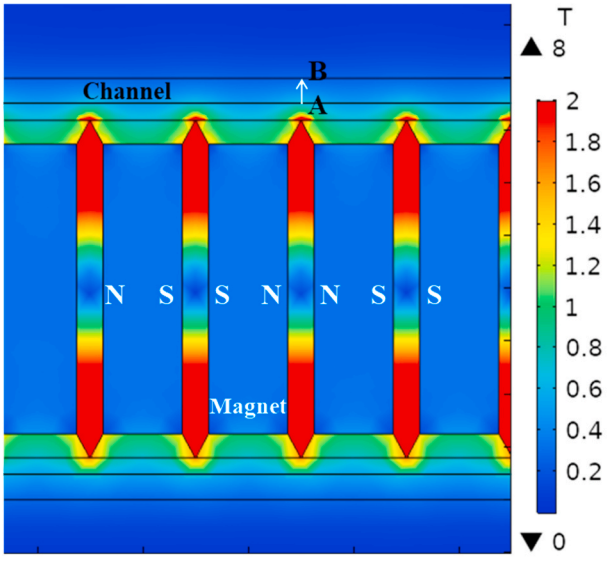

(b)

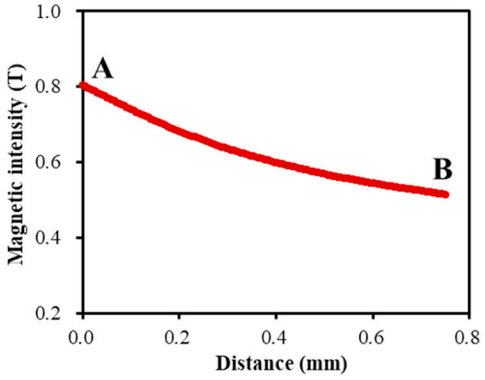

(c)

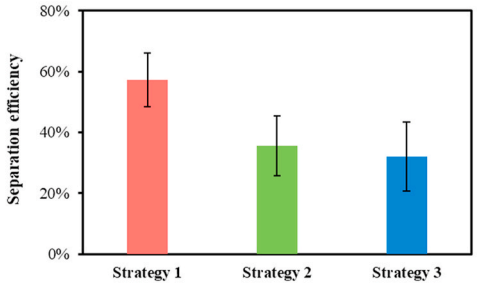

(d)

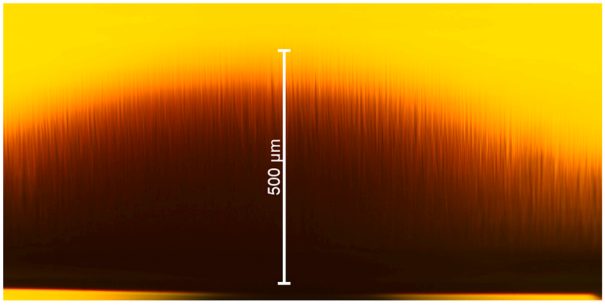

(e)

Fig. 2. (a) The forming mechanism of the MNB net. (b) The simulation on the distribution of the magnetic field using COMSOL software. (c) The vertical distribution of the magnetic field in the channel. (d) The comparison on three strategies for separation of *Salmonella* at a concentration of 10^3 CFU/mL (N = 3). (e) Microscopic image of the MNB net in the channel.

the ring channel, the MNB first moves horizontally with an initial velocity (v_0) (at t_0 moment). Due to the presence of the gradient magnetic field, the MNB is then dragged by the magnetic force (F_m) with the same direction as the magnetic field line from lower gradient zone to higher one along magnetic field lines (at t moment), and finally aggregate at the highest gradient zone (at t_1 moment). When the MNB hits the fixed one (gray), which has already been captured against the bottom wall, a counter force (F_c) in the reverse direction with the magnetic force starts to act on the MNB, making the MNB reach a balance. Thus, while the MNBs are continuously injected into the ring channel and the magnetic grid column is rotated, a MNB net is formed around the magnetic grid zone. To better understand the distribution of the magnetic field at the magnetic zone in the channel, the finite element analysis software COMSOL (Version 5.3a, Burlington, MA, USA) was used to simulate the magnetic field. As shown in Fig. 2(b-c), a high gradient magnetic field is generated in the channel at each tip of the iron grid with an average magnetic intensity of ~0.6 T and a mean gradient of ~380 T/m (from the inner wall, point A, to the outer wall, point B).

To evaluate the performance of the MNB nets for separation of target bacteria, this magnetic separation strategy with the MNB nets (Strategy 1: the MNBs were injected into the channel through the MNB locator) was compared with the one without the MNB nets (Strategy 2: the MNBs were inject into the channel through the inlet, see Fig. S3) and the conventional magnetic separation strategy in centrifuge tube (Strategy 3: the same amount of MNBs and the same reaction time were used) using 10 mL of *Salmonella* at the concentration of 10^3 CFU/mL. The waste was collected from the outlet, which was detected using the conventional culture plating method to obtain the number of unbound bacteria. Besides, the original bacterial sample was also detected using culture plating. The separation efficiency (SE) is calculated as the ratio of the difference between the number of the original bacteria (N_0) and that of the unbound bacteria (N_u) to N_0, i.e., $SE = (N_0 - N_u)/N_0$. As shown in Fig. 2(d), the separation efficiency for Strategy 1 (57% ± 8.9%) is obviously higher than those for Strategy 2 (36% ± 9.8%) and Strategy 3 (32% ± 11.4%). This is because longer MNB chains are formed in the ring channel through the locator (Strategy 1) to construct higher MNB nets, thus increasing the opportunity for the antibodies on the MNB nets to capture the flowing target bacteria. However, when the immune MNBs are directly injected (Strategy 2), they are aggregated at the inner wall of ring channel to construct shorter MNB nets, thus resulting in only partial MNBs on the top layer with the ability to capture the flowing bacteria. To further verify the forming of the MNB nets in the ring channel, a fluorescence inverted microscope (Nikon Eclipse Ti, Tokyo, Japan) was used to observe the MNB net from a side view after the MNBs were injected into the channel by the MNB locator (Fig. S4). As shown in Fig. 2(e), the MNB nets are successfully formed.

3.2. Mechanism of this impedance biosensor

To the best of our knowledge, this is the first time to investigate the feasibility of using H_2O_2 reduction of MnO_2 into Mn^{2+} for impedance biosensing of bacteria. Thus, it is of great importance to study the mechanism of this impedance biosensor. First of all, it is essential to verify the weak conductivity of H_2O_2 and the impedance change resulting from the reduction of MnO_2 into Mn^{2+}. Different concentrations of H_2O_2 ranging from 1 μM to 50 mM were prepared in deionized water and their electrochemical impedance spectra (EIS) were obtained using the microelectrode on the electrochemical station. As shown in Fig. 3(a), the electrochemical impedance spectra (EIS) for different concentrations of H_2O_2 basically overlaps that of deionized water, verifying the poor conductivity of H_2O_2. The impedance values for H_2O_2 with different concentrations at the characteristic frequency of 10 kHz are shown in Fig. 3(b) and have a relative standard deviation of 2.2%, indicating that their impedance doesn't change with their concentration, i.e., redundant H_2O_2 in the media does not have obvious impact on the impedance change. Besides, different concentrations of the MnO_2 NFs ranging from 0.01 to 0.40 mg/mL were decomposed by sufficient H_2O_2 (10 mM) for 30 min, and their EIS was conducted. As shown in Fig. 3(c-d), the impedance decreases when the concentration of MnO_2 NFs increases, this is because more Mn^{2+} ions are produced, thus resulting in better conductivity of the solution. A linear relationship between the impedance change (ΔZ) at the characteristic frequency of 10 kHz and the concentration of MnO_2 NFs (C) ranging from 0.01 to 0.40 mg/mL was obtained and can be described by $\Delta Z = 13{,}047*\ln(C) + 31{,}666$ ($R^2 = 0.99$).

To confirm the reduction of MnO_2 NFs into Mn^{2+} by H_2O_2, sodium bismuth oxide ($NaBiO_3$) was used as the indicator for the color development of Mn^{2+} because Mn^{2+} can specifically react with BiO_3^- in acidic condition to produce purplish-red MnO_4^-, resulting in the color change from colorless to purplish-red. As shown in Fig. 3(e), the purplish-red color becomes darker as more amount of MnO_2 NFs are decomposed by H_2O_2, while the color for MnO_2 NFs in deionized water (control) remains almost colorless even with 50 μg of MnO_2 NFs, verifying the reduction of MnO_2 NFs into Mn^{2+}.

3.3. Optimization of this impedance biosensor

The flowrate of the sample and the amount of the immune MNBs have great impact on the separation efficiency of target bacteria. Different flowrates (0.16, 0.4, 0.8 and 1.2 mL/min) were used to continuously inject the target bacteria with the concentration of 1.8×10^3 CFU/mL after the MNB nets were formed. As shown in Fig. 4(a), when the flowrate decreases from 1.2 to 0.4 mL/min, the separation efficiency of target bacteria gradually increases from 33% to 62%. However, further decrease to 0.16 mL/min only leads to ~5% increase in the separation efficiency. Thus, to trade off the separation efficiency and the separation time, the optimal flowrate of 0.4 mL/min was used in this study. Besides, different amounts of the immune MNBs were used to separate the target bacteria from 10 mL of target bacterial sample with the concentration of 1.5×10^4 CFU/mL at the optimal flowrate. As shown in Fig. 4(b), when the amount of the immune MNBs changes from 10 to 40 μg, the separation efficiency increases obviously from 17% to 62%. However, further increase to 50 μg only results in ~4% increase in the separation efficiency. Thus, the optimal amount of 40 μg for the immune MNBs was used in this study.

The concentration of H_2O_2 for decomposition of MnO_2, the time for H_2O_2 to react with MnO_2 and the amount of the immune MnO_2 NFs are important to the sensitivity of this biosensor. Different concentrations (20, 10, and 5 mM) of H_2O_2 were prepared and used to reduce the MNP-bacteria-MnO_2 complexes with the same bacterial concentration of 1.5×10^5 CFU/mL for 15 min. As shown in Fig. 4(c), when the concentration of H_2O_2 changes from 5 to 10 mM, the impedance change increases from 27,766 to 36,730 Ω. However, further increase to 20 mM does not result in obvious decrease (<2%) in the impedance, indicating that 10 mM is enough to completely decompose the MnO_2 NFs to Mn^{2+}. Thus, the optimal concentration of 10 mM for H_2O_2 was used in this study. Besides, different times (5, 10, 15 and 20 min) were used to decompose the MnO_2 NFs on the complexes by 500 μL of H_2O_2 at the optimal concentration of 10 mM. As shown in Fig. 4(d), when the time changes from 5 to 15 min, the impedance increases from 14,364 to 32,669 Ω. However, further increase to 20 min does not result in obvious increase (<5%) in the impedance change. To trade off the detection time and sensitivity, the optimal time of 15 min for MnO_2 NFs reduction was used in this study. Moreover, different amounts (50, 75, 100 and 125 μg) of the immune MnO_2 NFs were used to detect the target bacteria at the concentration of 4.2×10^6 CFU/mL. As shown in Fig. 4(e), when the amount changes from 50 to 100 μg, the impedance change increases from 20,823 to 45,407 Ω. However, further increase to 125 μg only results in 2% increase in the impedance change, indicating that 100 μg is sufficient for labeling the target bacteria with the concentrations of 10^6 CFU/mL or less. Thus, the optimal amount of 100 μg for the immune MnO_2 NFs was used in this study.

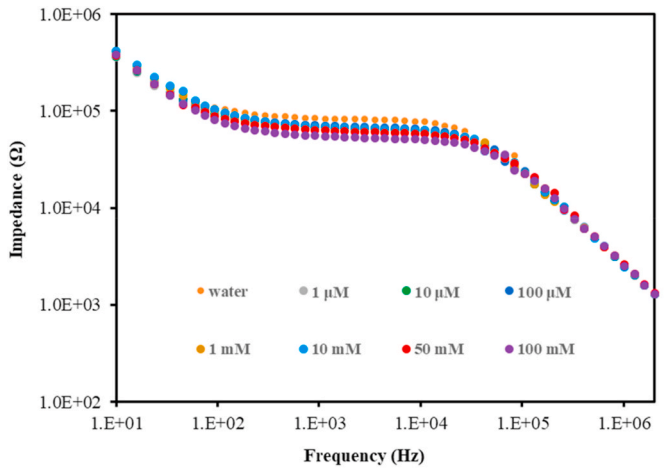

(a)

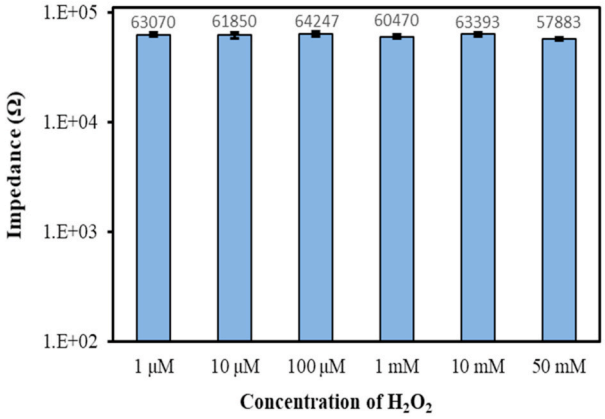

(b)

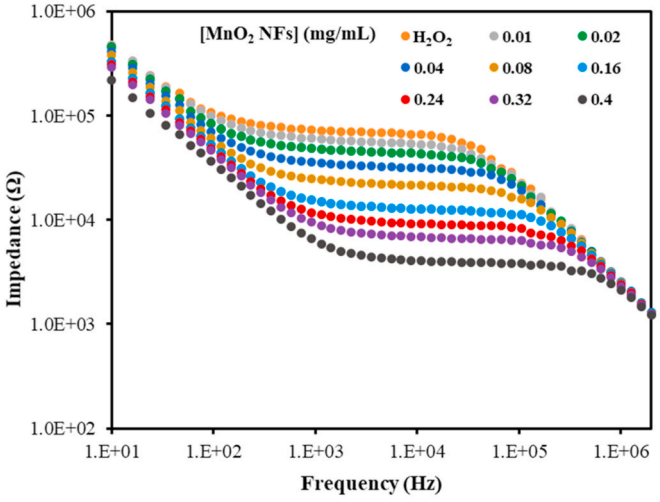

(c)

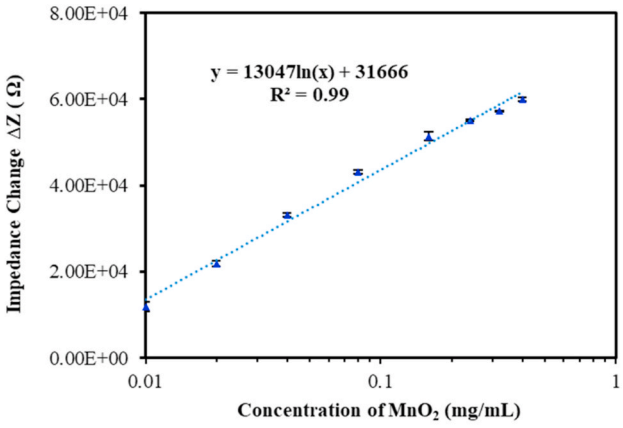

(d)

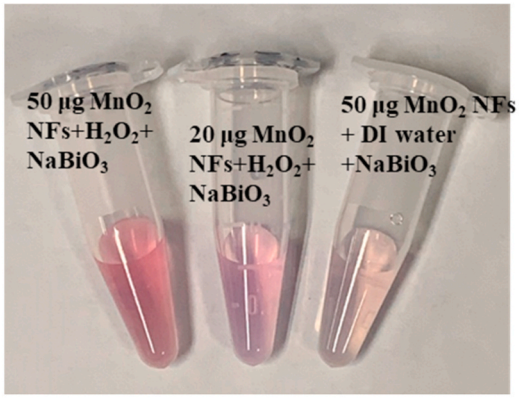

(e)

Fig. 3. (a) EIS of H_2O_2 with the concentrations of 1 μM–100 mM. (b) Impedance of H_2O_2 at the characteristic frequency of 10 kHz with the concentrations of 1 μM–50 mM (N = 3). (c) EIS of MnO_2 NFs with the concentration of 0.01 mg/mL to 0.40 mg/mL in H_2O_2 (10 mM). (d) Linear relationship between the impedance change at the characteristic frequency of 10 kHz and concentration of MnO_2 NFs (N = 3). (e) The color change for the reaction between Mn^{2+} and $NaBiO_3$. (For interpretation of the references to color in this figure legend, the reader is referred to the Web version of this article.)

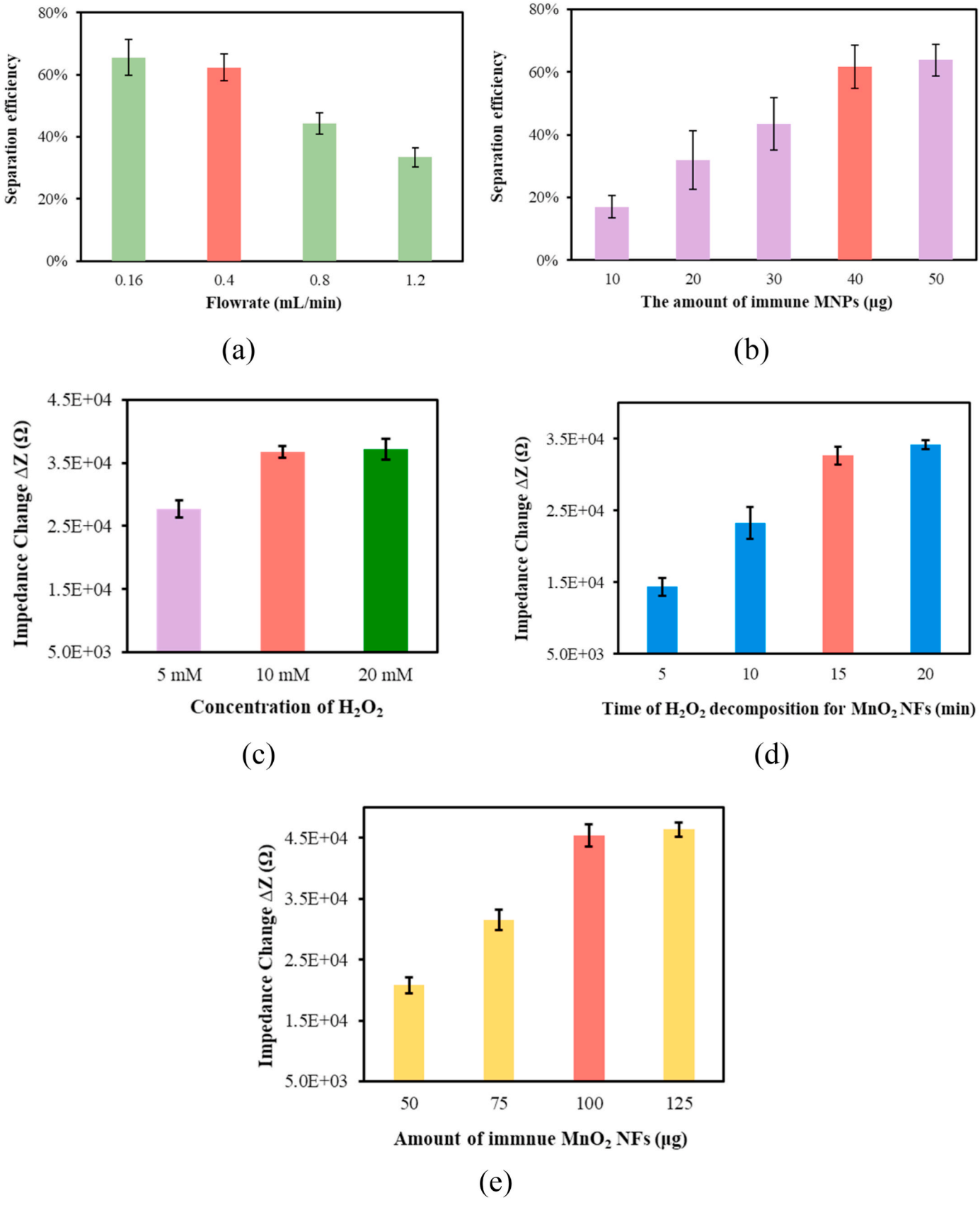

Fig. 4. Optimization of this biosensor: (a) The amount of the immune MNBs(N = 3). (b) The flowrate of the bacterial sample (N = 3). (c) The concentration of H_2O_2(N = 3). (d)The time for H_2O_2 to reduce MnO_2 NFs(N = 3). (e) The amount of the immune MnO_2 NFs(N = 3).

3.4. Sensitivity and specificity of this impedance biosensor

Under the optimal conditions, the calibration model between the impedance change and the concentration of target bacteria for this biosensor was established to determine the concentration of Salmonella in an unknown sample. Three parallel tests on pure *Salmonella* cells with different concentrations of 3.0×10^1–3.0×10^6 CFU/mL were conducted using this biosensor. As shown in Fig. 5(a), the impedance change at the frequency of 10 kHz increases from 10,892 to 44,638 Ω, while the bacterial concentration changes from 3.0×10^1 to 3.0×10^6 CFU/mL. A good linear relationship between the impedance change (ΔZ) and the concentration (C) is found in Fig. 5(b) and can be expressed by $\Delta Z = 6963.8*\log(C)+513.56$ ($R^2 = 0.98$). The lower detection limit was determined by 3 times of signal-to-noise ratio as 19 CFU/mL. Besides, the TEM imaging was used to verify the successful forming of MNB-bacteria-MnO_2 NFs complexes and shown in Fig. 5(c). This impedance biosensor was also compared with some recently reported methods for detection of bacteria. As shown in Table 1, this biosensor has shown a higher or comparable sensitivity and/or a shorter detection time. The high sensitivity of this biosensor was mainly contributed to the following aspects: (1) effective amplification of biological signals using the MnO_2 NFs as amplifying tags; (2) efficient separation of target bacteria from large volume (10 mL) of sample using the multiple MNB nets in the ring channel; (3) sensitive measurement of the impedance change using the microelectrode. More importantly, the forming of the MNB nets in the ring channel was controllable, which greatly enhanced the utilization efficiency of the immune MNBs and reduced the detection cost for each test.

To evaluate the specificity of this biosensor, four common foodborne pathogenic bacteria, including *Listeria*, *Staphylococcus*, *Bacillus* and *E. coli* with the concentration of 10^5 CFU/mL were used as non-target bacteria and detected using this biosensor. As shown in Fig. 5(d), it is obvious that the impedance change for target bacteria is much larger than those of non-target bacteria, verifying that this biosensor has a good specificity.

3.5. Detection of salmonella in spiked chicken meats

The practical applicability of this biosensor was evaluated by detecting the target bacteria in spiked chicken meat samples. The results were compared with the gold standard culture-plating method and shown in Table S1. The recoveries for chicken samples at concentrations of 5.0×10^1, 5.0×10^2, and 5.0×10^3 CFU/mL were 113.1%, 98.0%, and 94.5%, respectively, and the mean relative standard deviation of these samples were less than 8.5%. There was no significant difference between the readouts from this biosensor and those from the standard culture-plating method, indicating this biosensor had a good applicability for detection of *Salmonella* in chicken meat samples.

4. Conclusions

In this study, we have successfully developed a cost-effective impedance biosensor using self-assembled magnetic nanobead nets and MnO_2 nanoflowers for sensitive and rapid detection of *Salmonella*. This biosensor was able to quantitively detect *Salmonella* from 3.0×10^1 to 3.0×10^6 CFU/mL with the detection limit of 19 CFU/mL in 1.5 h. The immune MnO_2 NFs were verified to effectively amplify impedance signals and thus enhance the sensitivity of this biosensor. More importantly, the new magnetic nanobead net separator was demonstrated with satisfied separation efficiency (~60%) for target bacteria from a large volume (10 mL) of sample within a short time (~20 min) to improve the utilization ratio of magnetic nanobeads and the sensitivity of this biosensor. This biosensor might be further improved with higher sensitivity using larger volume of sample and used for routine screening of bacteria in foods with no need of bacterial pre-culture for 4–8 h.

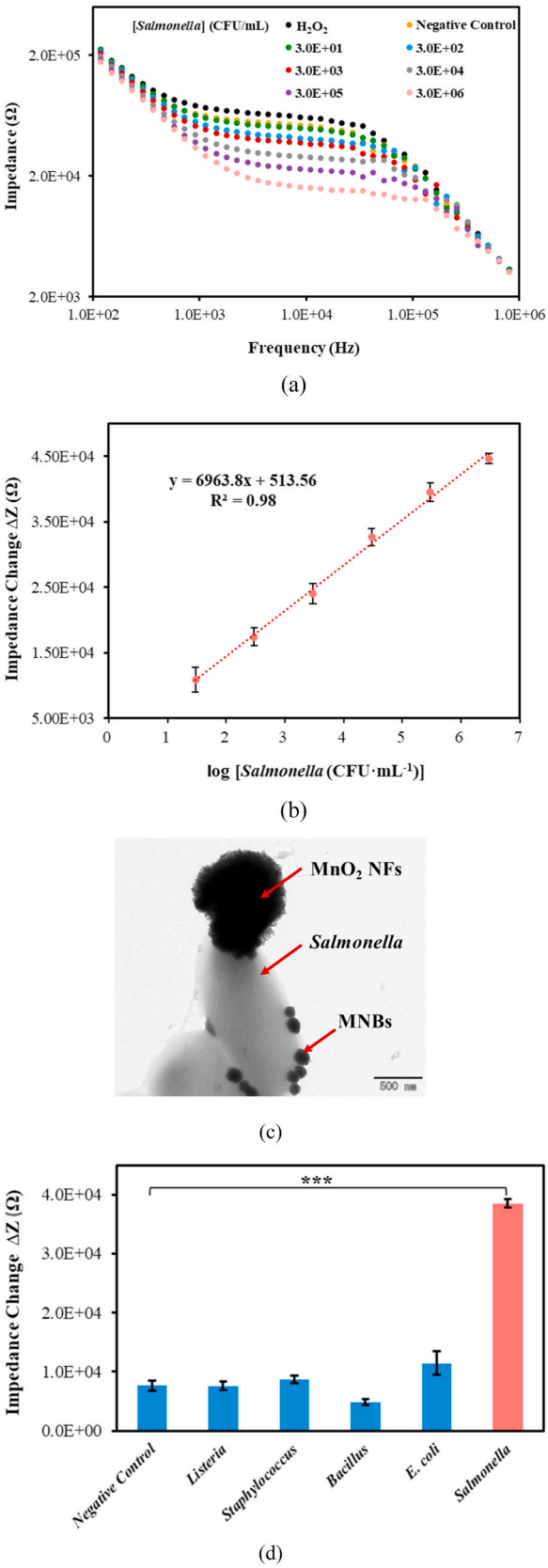

Fig. 5. (a) Electrochemical impedance spectra of *Salmonella* at the concentrations of 3.0×10^1–3.0×10^6 CFU/mL in the pure cultures; (b) Calibration curve of this biosensor for detection of *Salmonella* at the concentrations of 3.0×10^1–3.0×10^6 CFU/mL (N = 3); (c) TEM image of the MNB-bacteria-MnO_2 NFs complexes; (d) The specificity of the proposed biosensor to the non-target bacteria (N = 3) ***$p \leq 2.61 \times 10^{-5}$.

Table 1
Comparison of this biosensor with other reported methods for bacteria detection.

Methods	Sample volume (mL)	MNBs amount (mg)	LOD (CFU/mL)	Linear Range (CFU/mL)	Total time (h)	References
Photothermal	1.0	0.02	300	3.0×10^2–1.0×10^3	1.5	Zhang et al. (2018)
PCR[a]	10.0	0.7	8	8.0×10^0–8.0×10^4	7	Luo et al. (2017)
Fluorescent	0.4	0.5	16	3.2×10^1–1.0×10^8	4	Cheng et al. (2016)
Colorimetric	1.0	0.1	10^2	1.0×10^2–1.0×10^6	1.5	Srisa-Art et al. (2018)
ATP luminescent	10.0	3.0	100	–	0.25	Lee et al. (2019a)
Electrochemical	1.0	0.1	50	1.0×10^2–1.0×10^7	1	Zhu et al. (2020)
Impedance	1.0	1.0	10^2	1.0×10^2–1.0×10^6	–	Wang et al. (2020c)
Impedance	0.2	0.1	10^3	1.0×10^3–1.0×10^6	2	Xu et al. (2016)
Impedance	10.0	0.04	19	3.0×10^1–3.0×10^6	1.5	This study

[a] PCR: Immunomagnetic Separation Polymerase Chain Reaction.

CRediT authorship contribution statement

Li Xue: Conceptualization, Methodology, Data curation, Formal analysis, Project administration, Writing - original draft. **Ruya Guo:** Software, Data curation. **Fengchun Huang:** Methodology, Formal analysis. **Wuzhen Qi:** Software, Formal analysis. **Yuanjie Liu:** Formal analysis. **Gaozhe Cai:** Data curation. **Jianhan Lin:** Conceptualization, Formal analysis, Supervision, Project administration, Funding acquisition, Writing - review & editing.

Declaration of competing interest

The authors declare that they have no known competing financial interests or personal relationships that could have appeared to influence the work reported in this paper.

Acknowledgments

This study was supported in part by Chinese Universities Scientific Fund (2020TC116), Research Innovation Fund for Graduate Students of China Agricultural University (2020XYZC37A), and Fundamental Research Funds for the Central Universities of China (2019TC045).

Appendix A. Supplementary data

Supplementary data to this article can be found online at https://doi.org/10.1016/j.bios.2020.112800.

References

Abdelhaseib, M.U., Singh, A.K., Bailey, M., Singh, M., El-Khateib, T., Bhunia, A.K., 2016. Fiber optic and light scattering sensors: complimentary approaches to rapid detection of Salmonella enterica in food samples. Food Contr. 61, 135–145.
Armbrecht, L., Dincer, C., Kling, A., Horak, J., Kieninger, J., Urban, G., 2015. Self-assembled magnetic bead chains for sensitivity enhancement of microfluidic electrochemical biosensor platforms. Lab Chip 15 (22), 4314–4321.
Bezdekova, J., Zemankova, K., Hutarova, J., Kociova, S., Smerkova, K., Adam, V., Vaculovicova, M., 2020. Magnetic molecularly imprinted polymers used for selective isolation and detection of Staphylococcus aureus. Food Chem. 321, 126673.
Cesewski, E., Johnson, B.N., 2020. Electrochemical biosensors for pathogen detection. Biosens. Bioelectron. 112214.
Cheng, D., Yu, M., Fu, F., Han, W., Li, G., Xie, J., Song, Y., Swihart, M.T., Song, E., 2016. Dual recognition strategy for specific and sensitive detection of bacteria using aptamer-coated magnetic beads and antibiotic-capped gold nanoclusters. Anal. Chem. 88 (1), 820–825.
Du, H., Li, Z., Wang, Y., Yang, Q., Wu, W., 2020. Nanomaterial-based optical biosensors for the detection of foodborne bacteria. Food Rev. Int. 1–30.
Han, T., Zhu, S., Wang, S., Wang, B., Zhang, X., Wang, G., 2019. Fluorometric methods for determination of H2O2, glucose and cholesterol by using MnO2 nanosheets modified with 5-carboxyfluorescein. Mikrochim. Acta 186 (5), 269.
Helali, S., Sawelem Eid Alatawi, A., Abdelghani, A., 2018. Pathogenic Escherichia coli biosensor detection on chicken food samples. J. Food Saf. 38 (5), e12510.
Hou, Y., Tang, W., Qi, W., Guo, X., Lin, J., 2020. An ultrasensitive biosensor for fast detection of Salmonella using 3D magnetic grid separation and urease catalysis. Biosens. Bioelectron. 157, 112160.
Hu, J., Jiang, Y.Z., Tang, M., Wu, L.L., Xie, H.Y., Zhang, Z.L., Pang, D.W., 2019. Colorimetric-Fluorescent-magnetic nanosphere-based multimodal assay platform for Salmonella detection. Anal. Chem. 91 (1), 1178–1184.
Huang, F., Xue, L., Zhang, H., Guo, R., Li, Y., Liao, M., Wang, M., Lin, J., 2018a. An enzyme-free biosensor for sensitive detection of Salmonella using curcumin as signal reporter and click chemistry for signal amplification. Theranostics 8 (22), 6263–6273.
Huang, F., Zhang, H., Wang, L., Lai, W., Lin, J., 2018b. A sensitive biosensor using double-layer capillary based immunomagnetic separation and invertase-nanocluster based signal amplification for rapid detection of foodborne pathogen. Biosens. Bioelectron. 100, 583–590.
Huang, Z., Yang, J., Zhang, L., Geng, X., Ge, J., Hu, Y., Li, Z., 2017. A novel one-step colorimetric assay for highly sensitive detection of glucose in serum based on MnO2 nanosheets. Analytical Methods 9 (29), 4275–4281.
Jasim, I., Shen, Z., Mlaji, Z., Yuksek, N.S., Abdullah, A., Liu, J., Dastider, S.G., El-Dweik, M., Zhang, S., Almasri, M., 2019. An impedance biosensor for simultaneous detection of low concentration of Salmonella serogroups in poultry and fresh produce samples. Biosens. Bioelectron. 126, 292–300.
Jung, S.H., Hahn, Y.K., Oh, S., Kwon, S., Um, E., Choi, S., Kang, J.H., 2018. Advection flows-enhanced magnetic separation for high-throughput bacteria separation from undiluted whole blood. Small 14 (34), e1801731.
Jung, T., Jung, Y., Ahn, J., Yang, S., 2020. Continuous, rapid concentration of foodborne bacteria (Staphylococcus aureus, Salmonella typhimurium, and Listeria monocytogenes) using magnetophoresis-based microfluidic device. Food Contr. 114, 107229.
Lee, H., Kim, G., Park, E., Jeon, S., 2019a. Lenz's law-based virtual net for detection of pathogenic bacteria from water. Anal. Chem. 91 (24), 15585–15590.
Lee, P.C., Li, N.S., Hsu, Y.P., Peng, C., Yang, H.W., 2019b. Direct glucose detection in whole blood by colorimetric assay based on glucose oxidase-conjugated graphene oxide/MnO2 nanozymes. Analyst 144 (9), 3038–3044.
Lee, W., Kwon, D., Chung, B., Jung, G.Y., Au, A., Folch, A., Jeon, S., 2014. Ultrarapid detection of pathogenic bacteria using a 3D immunomagnetic flow assay. Anal. Chem. 86 (13), 6683–6688.
Luo, D., Huang, X., Mao, Y., Chen, C., Li, F., Xu, H., Xiong, Y., 2017. Two-step large-volume magnetic separation combined with PCR assay for sensitive detection of Listeria monocytogenes in pasteurized milk. J. Dairy Sci. 100 (10), 7883–7890.
Mathelié-Guinlet, M., Cohen-Bouhacina, T., Gammoudi, I., Martin, A., Béven, L., Delville, M.-H., Grauby-Heywang, C., 2019. Silica nanoparticles-assisted electrochemical biosensor for the rapid, sensitive and specific detection of Escherichia coli. Sensor. Actuator. B Chem. 292, 314–320.
Ouyang, H., Lu, Q., Wang, W., Song, Y., Tu, X., Zhu, C., Smith, J.N., Du, D., Fu, Z., Lin, Y., 2018. Dual-readout immunochromatographic assay by utilizing MnO2 nanoflowers as the unique colorimetric/chemiluminescent probe. Anal. Chem. 90 (8), 5147–5152.
Pang, B., Zhao, C., Li, L., Song, X., Xu, K., Wang, J., Liu, Y., Fu, K., Bao, H., Song, D., Meng, X., Qu, X., Zhang, Z., Li, J., 2018. Development of a low-cost paper-based ELISA method for rapid Escherichia coli O157:H7 detection. Anal. Biochem. 542, 58–62.
Pastucha, M., Farka, Z., Lacina, K., Mikusova, Z., Skladal, P., 2019. Magnetic nanoparticles for smart electrochemical immunoassays: a review on recent developments. Mikrochim. Acta 186 (5), 312.
Shan, S., Liu, D., Guo, Q., Wu, S., Chen, R., Luo, K., Hu, L., Xiong, Y., Lai, W., 2016. Sensitive detection of Escherichia coli O157:H7 based on cascade signal amplification in ELISA. J. Dairy Sci. 99 (9), 7025–7032.
Shu, Y., Xu, J., Chen, J., Xu, Q., Xiao, X., Jin, D., Pang, H., Hu, X., 2017. Ultrasensitive electrochemical detection of H2O2 in living cells based on ultrathin MnO2 nanosheets. Sensor. Actuator. B Chem. 252, 72–78.
Srisa-Art, M., Boehle, K.E., Geiss, B.J., Henry, C.S., 2018. Highly sensitive detection of Salmonella typhimurium using a colorimetric paper-based analytical device coupled with immunomagnetic separation. Anal. Chem. 90 (1), 1035–1043.
Wang, L., Huo, X., Zheng, L., Cai, G., Wang, Y., Liu, N., Wang, M., Lin, J., 2020a. An ultrasensitive biosensor for colorimetric detection of Salmonella in large-volume sample using magnetic grid separation and platinum loaded zeolitic imidazolate Framework-8 nanocatalysts. Biosens. Bioelectron. 150, 111862.
Wang, L., Xue, L., Guo, R., Zheng, L., Wang, S., Yao, L., Huo, X., Liu, N., Liao, M., Li, Y., Lin, J., 2020b. Combining impedance biosensor with immunomagnetic separation for rapid screening of Salmonella in poultry supply chains. Poultry Sci. 99 (3), 1606–1614.
Wang, S., Sun, C., Hu, Q., Li, S., Wang, C., Wang, P., Zhou, L., 2020c. A homogeneous magnetic bead-based impedance immunosensor for highly sensitive detection of Escherichia coli O157:H7. Biochem. Eng. J. 156, 107513.

Xianyu, Y., Wu, J., Chen, Y., Zheng, W., Xie, M., Jiang, X., 2018. Controllable assembly of enzymes for multiplexed lab-on-a-chip bioassays with a tunable detection range. Angew Chem. Int. Ed. Engl. 57 (25), 7503–7507.
Xu, M., Wang, R., Li, Y., 2016. Rapid detection of Escherichia coli O157:H7 and Salmonella Typhimurium in foods using an electrochemical immunosensor based on screen-printed interdigitated microelectrode and immunomagnetic separation. Talanta 148, 200–208.
Xu, Z., Teng, H., Song, J., Gao, F., Ma, L., Xu, G., Luo, X., 2019. A nanocomposite consisting of MnO2 nanoflowers and the conducting polymer PEDOT for highly sensitive amperometric detection of paracetamol. Mikrochim. Acta 186 (8), 499.
Xue, L., Huang, F., Hao, L., Cai, G., Zheng, L., Li, Y., Lin, J., 2020. A sensitive immunoassay for simultaneous detection of foodborne pathogens using MnO2 nanoflowers-assisted loading and release of quantum dots. Food Chem. 322, 126719.
Xue, L., Zheng, L., Zhang, H., Jin, X., Lin, J., 2018. An ultrasensitive fluorescent biosensor using high gradient magnetic separation and quantum dots for fast detection of foodborne pathogenic bacteria. Sensor. Actuator. B Chem. 265, 318–325.
Yang, H., Li, P., Wang, D., Liu, Y., Wei, W., Zhang, Y., Liu, S., 2019. Quartz crystal microbalance detection of poly(ADP-ribose) polymerase-1 based on gold nanorods signal amplification. Anal. Chem. 91 (17), 11038–11044.
Zhang, J., Dai, X., Song, Z.-L., Han, R., Ma, L., Fan, G.-C., Luo, X., 2020. One-pot enzyme- and indicator-free colorimetric sensing of glucose based on MnO2 nano-oxidizer. Sensor. Actuator. B Chem. 304, 127304.
Zhang, Y., Hu, K., Ling, Z., Di, W., 2019. A MnO2–[Ru(dpp)3]Cl2 system for colorimetric and fluorimetric dual-readout detection of H2O2. RSC Adv. 9 (14), 7803–7810.
Zhang, Z., Wang, Q., Han, L., Du, S., Yu, H., Zhang, H., 2018. Rapid and sensitive detection of Salmonella typhimurium based on the photothermal effect of magnetic nanomaterials. Sensor. Actuator. B Chem. 268, 188–194.
Zhou, B., Chen, B., Wu, X., Li, F., Yu, P., Aguilar, Z.P., Wei, H., Xu, H., 2016. A new application of a sodium deoxycholate-propidium monoazide-quantitative PCR assay for rapid and sensitive detection of viable Cronobacter sakazakii in powdered infant formula. J. Dairy Sci. 99 (12), 9550–9559.
Zhu, W., Chen, Y., He, Y., Fang, W., Ying, Y., Li, Y., Fu, Y., 2020. Cooperation mode of outer surface and inner space of nanochannel: separation-detection system based on integrated nanochannel electrode for rapid and facile detection of Salmonella. Anal. Chem. 92 (2), 1818–1825.